VORTEX DYNAMICS

1. Introduction

A vortex is commonly associated with the rotating motion of fluid around a common centerline. It is defined by the *vorticity* in the fluid, which measures the rate of local fluid rotation. Typically, the fluid circulates around the vortex, the speed increases as the vortex is approached and the pressure decreases. Vortices arise in nature and technology in a large range of sizes as illustrated by the examples given in Table 1. The next section presents some of the mathematical background necessary to understand vortex formation and evolution. Section 3 describes sample flows, including important instabilities and reconnection processes. Section 4 presents some of the numerical methods used to simulate these flows.

Vortex	Diameter
superfluid vortices	10^{-8} cm (= 1Å)
trailing vortex of Boeing 727	1–2 m
dust devils	1–10 m
tornadoes	10–500 m
hurricanes	100–2000 km
Jupiter's Red Spot	25,000 km
spiral galaxies	thousands of light years

TABLE 1: Sample vortices and typical sizes.

2. Background

Let D be a region in 3D space containing a fluid, and let $\mathbf{x} = (x, y, z)^T$ be a point in D. The fluid motion is described by its velocity $\mathbf{u}(\mathbf{x}, t) = u(\mathbf{x}, t)\mathbf{i} + v(\mathbf{x}, t)\mathbf{j} + w(\mathbf{x}, t)\mathbf{k}$, and depends on the fluid density $\rho(\mathbf{x}, t)$, temperature $T(\mathbf{x}, t)$, gravitational field $\mathbf{g}$ and other external forces possibly acting on it. The fluid vorticity is defined by $\boldsymbol{\omega} = \nabla \times \mathbf{u}$. The vorticity measures the local fluid rotation about an axis, as can be seen by expanding the velocity near $\mathbf{x} = \mathbf{x}_0$,

$$\mathbf{u}(\mathbf{x}) = \mathbf{u}(\mathbf{x}_0) + D(\mathbf{x}_0)(\mathbf{x} - \mathbf{x}_0) + \frac{1}{2}\boldsymbol{\omega}(\mathbf{x}_0) \times (\mathbf{x} - \mathbf{x}_0) + O(|\mathbf{x} - \mathbf{x}_0|^2) \quad (1)$$

where

$$D(\mathbf{x}_0) = \frac{1}{2}(\nabla\mathbf{u} + \nabla\mathbf{u}^T), \nabla\mathbf{u} = \begin{bmatrix} u_x & u_y & u_z \\ v_x & v_y & v_z \\ w_x & w_y & w_z \end{bmatrix} . \quad (2)$$

The first term $\mathbf{u}(\mathbf{x}_0)$ corresponds to translation: all fluid particles move with constant velocity $\mathbf{u}(x_0)$. The second term $D(\mathbf{x}_0)(\mathbf{x} - \mathbf{x}_0)$ corresponds to a strain field in the three directions of the eigenvectors of the symmetric matrix D. If the eigenvalue corresponding to a given eigenvector is positive, the fluid is stretched in that direction, if it is negative, the fluid is compressed. Note that in incompressible flow $\nabla \cdot \mathbf{u} = 0$, so the sum of the eigenvalues of D equals zero.

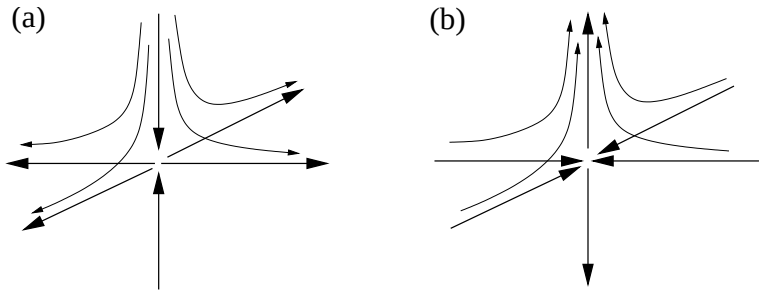

Figure 1: Strainfield. (a) Two positive eigenvalues, sheet formation. (b) One positive eigenvalue, tube formation.

Thus at least one eigenvalue is positive and one negative. If the third eigenvalue is positive, fluid particles move towards sheets (Fig. 1a). If the third eigenvalue is negative, fluid particles move towards tubes (Fig. 1b). The last term in Eq. (1), $\frac{1}{2}\boldsymbol{\omega}(\mathbf{x}_0) \times (\mathbf{x} - \mathbf{x}_0)$, corresponds to a rotation: near a point with $\boldsymbol{\omega}(\mathbf{x}_0) \neq 0$, the fluid rotates with angular velocity $|\boldsymbol{\omega}|/2$ in a plane normal to the vorticity vector $\boldsymbol{\omega}$. Fluid for which $\boldsymbol{\omega} = \mathbf{0}$ is said to be *irrotational*.

A *vortex line* is an integral curve of the vorticity. For incompressible flow, $\nabla \cdot \boldsymbol{\omega} = \nabla \cdot (\nabla \times \mathbf{u}) = 0$ which implies that vortex lines cannot end in the interior of the flow, but must either form a closed loop or start and end at a bounding surface. In 2D flow, $\mathbf{u} = u\mathbf{i} + v\mathbf{j}$ and the vorticity is $\boldsymbol{\omega} = \omega\mathbf{k}$, where $\omega = v_x - u_y$ is the *scalar vorticity*. Thus in 2D, the vorticity points in the z-direction and the vortex lines are straight lines normal to the x-y plane. A *vortex tube* is a bundle of vortex lines. The *strength* of a vortex tube is defined as the *circulation* $\int_C \mathbf{u} \cdot d\mathbf{s}$ about a curve C enclosing the tube. By Stokes' Theorem,

$$\int_C \mathbf{u} \cdot d\mathbf{s} = \int\int_A \boldsymbol{\omega} \cdot \mathbf{n} dS \ , \tag{3}$$

and thus the circulation can also be interpreted as the flux of vorticity through a cross section of the tube. In inviscid incompressible flow of constant density, *Helmholtz' Theorem* states that the tube strength is independent of the curve C, and is therefore a well-defined quantity, and *Kelvin's Theorem* states that a tube's strength remains constant in time. A *vortex filament* is an idealization in which a tube is represented by a single vortex line of nonzero strength.

The evolution equation for the fluid vorticity, as derived from the Navier-Stokes Equations, is

$$\frac{\mathrm{d}\boldsymbol{\omega}}{\mathrm{d}t} = \boldsymbol{\omega} \cdot \nabla \mathbf{u} + \nu \Delta \boldsymbol{\omega} \tag{4}$$

where $\mathrm{d}/\mathrm{d}t = \partial/\partial t + \mathbf{u} \cdot \nabla$ is the total time derivative. Equation (4) states that the vorticity is transported by the fluid velocity (first term), stretched by the fluid velocity gradient (second term), and diffused by viscosity ν (last term). These equations are usually nondimensionalized and written in terms of the Reynolds number, a dimensionless quantity inversely proportional to viscosity.

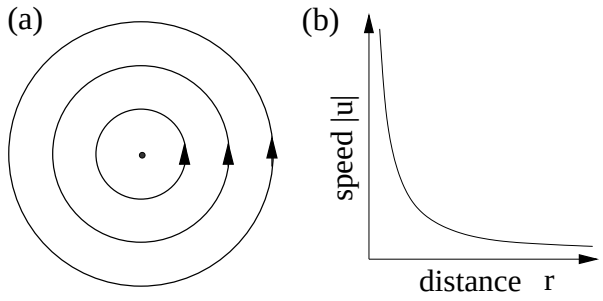

Figure 2: Flow induced by a point vortex. (a) Streamlines. (b) Speed $|\mathbf{u}|$ vs. distance r.

To understand high Reynolds number flow it is of interest to study the inviscid Euler Equations. The corresponding vorticity evolution equation in 2D is

$$\frac{\mathrm{d}\boldsymbol{\omega}}{\mathrm{d}t} = 0 \ , \tag{5}$$

which states that 2D vortex filaments in inviscid flow move with the fluid velocity. Furthermore, in incompressible flow the fluid velocity is determined by the vorticity, up to an irrotational far-field component $\mathbf{u}_\infty$, through the *Biot-Savart law*,

$$\mathbf{u}(\mathbf{x}) = -\frac{1}{4\pi}\int \frac{(\mathbf{x}-\mathbf{x}')\times\boldsymbol{\omega}(\mathbf{x}')}{|\mathbf{x}-\mathbf{x}'|^3}d\mathbf{x}' + \mathbf{u}_\infty \ . \tag{6}$$

In planar 2D flow, Eq (6) reduces to

$$\mathbf{u}(\mathbf{x}) = \mathbf{K}_{2d} * \omega, \text{where } \mathbf{K}_{2d}(\mathbf{x}) = \frac{1}{2\pi}\frac{-y\mathbf{i}+x\mathbf{j}}{|\mathbf{x}|^2} \tag{7}$$

and $\omega(\mathbf{x})$ is the scalar vorticity. Equations (4,5) and (6,7) are the basis of the numerical methods discussed in §4.

A *vortex* is typically defined by a region in the fluid of concentrated vorticity. A simple model is a *point vortex* in 2D flow, which corresponds to a straight vortex filament of unit circulation. The associated scalar vorticity is a delta function in the plane, and the induced velocity is obtained from the Biot-Savart law. For a point vortex at the origin this reduces to the radial velocity field $\mathbf{u}(\mathbf{x}) = \mathbf{K}_{2d} * \delta = \mathbf{K}_{2d}(\mathbf{x})$. Corresponding particle trajectories are shown in Fig. 2(a). The particle speed $|\mathbf{u}| = 1/r$ increases unboundedly as the vortex center is approached, and vanishes as $r \to \infty$ (Fig. 2b). In general, the far field velocity of a concentrated vortex behaves similarly to the one of a point vortex, with speeds decaying as $1/r$. Near the vortex center, the velocity typically increases in magnitude and as a result, the fluid pressure decreases (*Bernoulli's Theorem*). A vortex of arbitrary shape can be approximated by a sum of point vortices (in 2D) or vortex filaments (in 3D), as is often done for simulation purposes.

Vorticity can be generated by a variety of mechanisms. For example, vorticity can be generated by density gradients, which in turn are induced by spatial

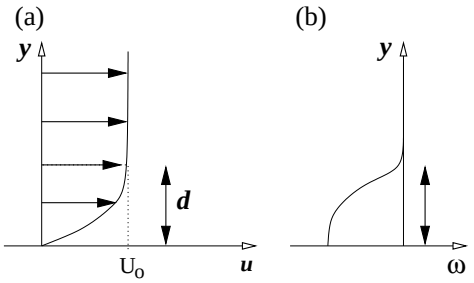

Figure 3: Velocity and vorticity in boundary layer near a flat wall.

temperature variations. This mechanism explains the formation of warm-air vortices when a layer of hot air is trapped underneath cooler air. Vorticity is also generated near solid walls in the form of *boundary layers* caused by viscosity. To illustrate, imagine horizontal flow with speed U_o moving past a solid wall at rest (Fig. 3a). Since in viscous flow the fluid sticks to the wall (the no-slip boundary condition), the fluid velocity at the wall is zero. As a result, there is a thin layer near the wall in which the horizontal velocity varies greatly while the vertical velocity gradients are small, yielding large negative vorticity values $\omega = v_x - u_y$ (Fig. 3b). Similarity solutions to the approximating *Prandtl boundary layer equations* show that the boundary layer thickness d grows proportional to $\sqrt{t}$ where t measures the time from the beginning of the motion. Boundary layers can separate from the wall at corners or regions of high curvature and move into the fluid interior, as illustrated in several of the following examples.

3. Sample vortex flows

3.1 Shear layers

A shear layer is a thin region of concentrated vorticity across which the tangential velocity component varies greatly. An example is the constant vorticity layer given by parallel 2D flow $u(x, y) = U(y)$, $v(x, y) = 0$, where U is as shown in Fig. 4(a). In this case, the velocity is constant outside the layer and linear inside. The vorticity $\omega = -U'(y)$ is zero outside the layer and constant inside. Shear layers occur naturally in the ocean or atmosphere when regions of distinct temperature or density meet. To illustrate this scenario, consider a tank containing two horizontal layers of fluids of different densities, one on top of the other. If the tank is tilted, the heavier bottom fluid moves downstream, and the lighter one moves upstream, creating a shear layer.

Flat shear layers are unstable to perturbations: they do not remain flat but roll up into a sequence of vortices. This is the *Kelvin-Helmholtz instability*, which can be deduced analytically using linear stability analysis. One shows that in a periodically perturbed flat shear layer, the amplitude of a perturbation with wavenumber k will initially grow exponentially in time as e^{wt}, where $w = w(k)$ is the *dispersion relation*, leading to instability. The wavenumber of largest growth depends on the layer thickness. This is illustrated in Fig. 4(b), which

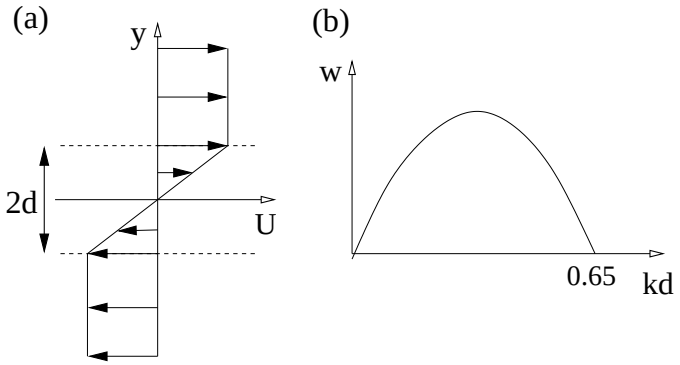

Figure 4: Shear layer. (a) Velocity profile. (b) Dispersion relation.

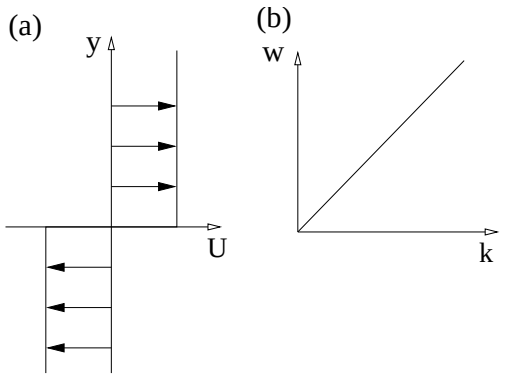

Figure 5: Vortex sheet. (a) Velocity profile. (b) Dispersion relation.

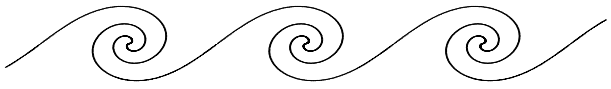

Figure 6: Computation of vortex sheet roll-up.

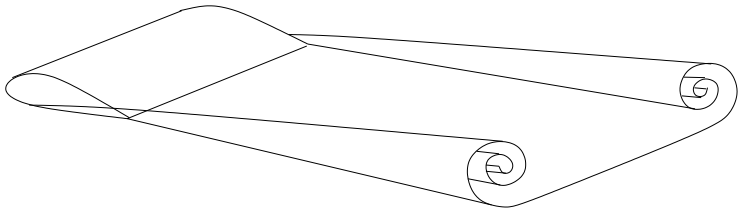

Figure 7: Sketch. Shear layer separation and roll-up into trailing vortices behind an airfoil.

plots $w(k)$ for a constant vorticity layer of thickness $2d$. The wavenumber of maximal growth is proportional to $1/d$.

A vortex sheet is a model for a shear layer. The layer is approximated by a surface of zero thickness across which the tangential velocity is discontinuous, as illustrated in Fig. 5(a). In this case the dispersion relation reduces to $w(k) = \pm k$. That is, for each wavenumber k there is a growing and a decaying mode, and the growing mode grows faster the higher the wavenumber is, as shown in Fig. 5(b). The vortex sheet arises from a constant vorticity shear layer as the thickness $d \to 0$ and the vorticity $\omega \to \infty$ in such a way that the product $\omega\, d$ remains constant. Figure 6 shows the roll-up of a periodically perturbed vortex sheet due to the Kelvin-Helmholtz instability, computed using one of the methods described in §4.

3.2 Aircraft trailing vortices

One can often observe trailing vortices that shed from the wings of a flying aircraft (also called contrails). These vortices are formed because the wing develops lift. The pressure on the top of the wing is lower than on bottom, causing air to move around the edge of the wing from the bottom surface to the top. The boundary layer on the wing separates as a shear layer that rolls up into a vortex attached to the tip of the wing (Fig. 7). Since the velocity inside the vortex is high, the pressure is correspondingly low and causes water vapor in the air to condense, forming water droplets that visualize the vortices. The vortex strength increases with increasing lift, and is particularly strong in high-lift conditions such as take-off and landing. Since lift is proportional to weight, it also increases with the size of the airplane. Vortices of large planes are strong enough to flip a small one if it gets too close. Trailing vortices are the principal reason for the time delay between take-off and landing and are still a serious issue for crowded urban airports.

The trailing vortices can be modelled by a pair of counter-rotating vortex lines (Fig. 8a). Two parallel vortex lines of opposite strength induce a downward motion on each other, similar to two point vortices, the zero core limit. Two point vortices of strength $\pm\Gamma$ at a distance $2d$ from each other translate with

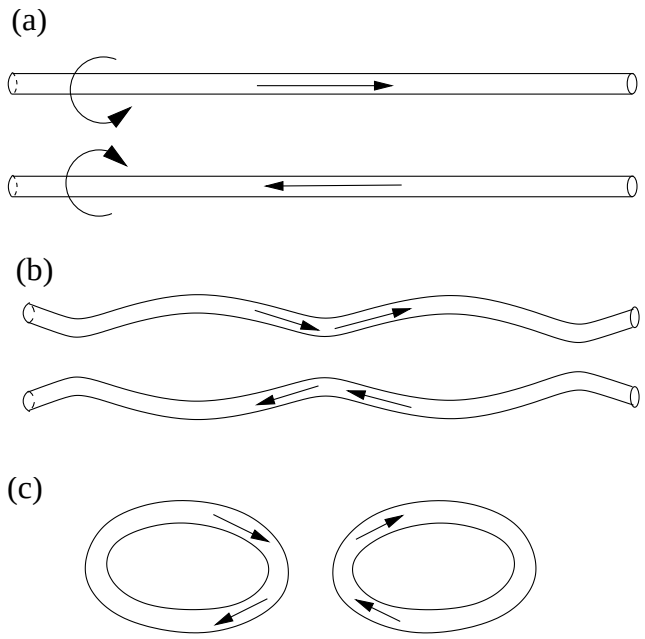

Figure 8: Sketch. Onset of Crow instability in a pair of vortex lines and ensuing reconnection.

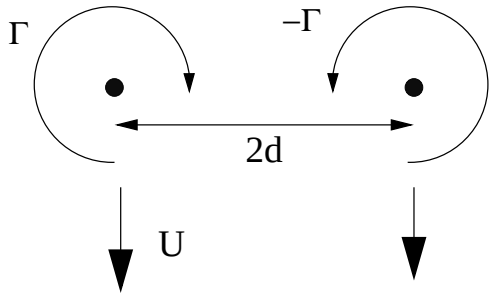

Figure 9: Self-induced downward motion of a vortex pair.

self-induced velocity

$$U = \frac{\Gamma}{4\pi d} \tag{8}$$

(Fig. 9). As a result trailing vortices near takeoff hit the ground as a strong downwash air current.

Vortex decay results generally from the development of instabilities. Two parallel vortex tubes are subject to the long-wavelength *Crow instability*. Triggered by turbulence in the surrounding air, or by local variations in air temperature or density, the vortices develop symmetric sinusoidal perturbations with long wavelength, of the same order as the vortex separation (Fig. 8b). As the perturbations grow to finite amplitude the tubes reconnect and produce a sequence of vortex rings. Note that the two-dimensional schematic in Fig. 8c does not convey the three-dimensional structure of the rings. The reconnection process destroys the initial wake structure more rapidly than viscous decay of the individual filaments.

Of much interest is the study of how to accelerate the vortex decay. High aspect ratio vortices are subject to a shorter wavelength elliptic instability, which leads to earlier destruction. However, such vortices are not realistic in current aircraft wakes. Wing designs have been proposed in which more that two trailing vortices form which interact strongly and lead to faster decay. Other interesting aspects are the effect of ambient turbulence and vortex breakdown. Breakdown refers to a disturbance in the vortex core in which it quickly, within an axial distance of few core diameters, develops a region of reversed flow and loses its laminar behaviour.

Unlike the counterrotating vortices discussed so far, two equally signed vortices rotate under their self-induced velocity about a common axis. If the separation distance between them is too small, two equally signed patches merge into one. Vortex merging occurs in two- or three-dimensional flows, as opposed to vortex reconnection, which is a strictly three-dimensional phenomenon.

3.3 Vortex rings

A vortex tube that forms a closed loop is called a vortex ring. Vortex rings can be formed by ejecting fluid from a circular opening, such as when a smoke ring is formed. The boundary layer wall vorticity separates at the opening as a cylindrical shear layer that rolls up at its edge into a ring (Fig. 10). The vorticity is concentrated in a core, which may be thin or thick relative to the ring diameter. The limiting cases are an infinitely thin circular filament of nonzero circulation and the *Hill's vortex*, in which the vorticity occupies all the interior of a sphere.

Just as a conterrotating vortex pair, a ring translates under its self-induced velocity U in direction normal to the plane of the ring (Fig. 11). However, unlike the vortex pair, the ring velocity depends significantly on its core thickness. For a ring with radius, circulation and core size R, Γ, a, the self-induced velocity is

$$U \sim \frac{\Gamma}{4\pi R}\Big(\log\frac{8R}{a} - \frac{1}{4}\Big)\ , \tag{9}$$

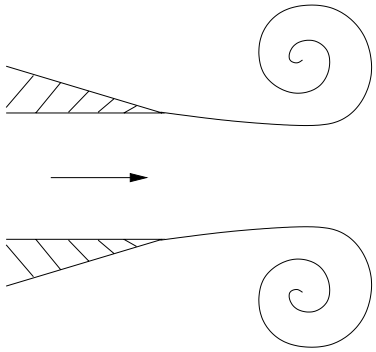

Figure 10: Vortex ring, formed by ejecting fluid from a circular tube.

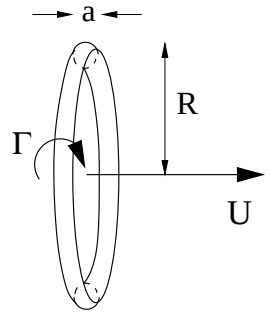

Figure 11: Self-induced motion of a vortex ring.

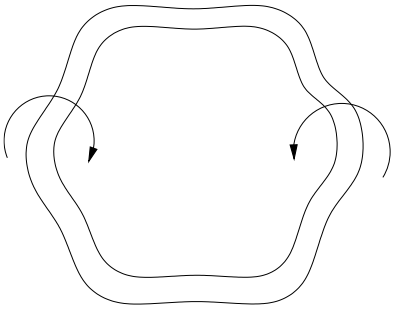

Figure 12: Sketch. Onset of azimuthal vortex ring instability.

asymptotically as $a \to 0$. Thus, the translation velocity becomes unbounded for rings with decreasing core size. In reality, at some point viscosity takes over and spreads the core vorticity, slowing the ring down.

Vortex rings of small cross-section are subject to an *azimuthal instability*. Theory, experiment and simulations show that if a ring is perturbed in the azimuthal direction, there exists a dominant wavenumber which is unstable and grows (Fig. 12). The unstable wavenumber increases as the core size decreases, while its spatial amplification rate is almost independent of the core size.

Interesting dynamics are obtained when two or more rings interact. Two coaxial vortex rings of equally signed circulation move in the same direction and exhibit leap-frogging: the rear ring causes the front ring to grow in radius and the front ring causes the rear one to decrease. From Eq. (9) it can be seen that the ring velocity is inversely proportional to its radius. Consequently, the front ring slows down and the rear ring speeds up, until the rear ring travels through the front ring. This process repeats itself and is known as leap-frogging. On the other hand, two coaxial vortex rings of oppositely signed circulation approach each other and grow in radius. Their cores contract in order to preserve volume, and their vorticity increases in order to preserve circulation. Under certain experimental conditions, the azimuthal instability develops, the resulting waves on opposite rings reconnect and a sequence of smaller rings form.

3.4 Vortices, mixing and chaos

Mixing is important in many natural processes and technological applications. For example, mixing in shear flows and wakes is relevant to aeronautics and combustion, mixing and diffusion determine chemical reaction rates, mixing of contaminants pollutes oceans and atmosphere. It is therefore important to understand and control mixing processes.

Efficient mixing of two fluids is obtained by efficient stretching and folding of material lines. Stretching and folding in turn are the fingerprint of chaos, thus mixing and chaos are intimately related. Mixing and associated chaotic fluid motion can be obtained by simple vortical motion. For example, two counterrotating vortices subject to a periodic strainfield oscillate in a regular

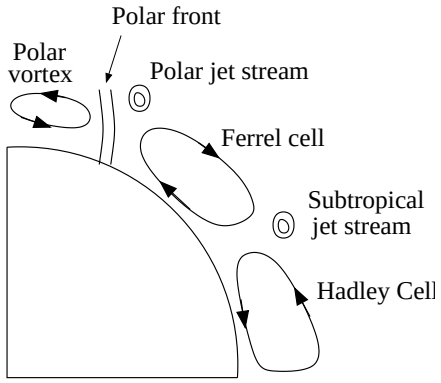

Figure 13: Vortices in the atmosphere.

fashion but induce chaos in a region of fluid moving with them. Similarly, two corotating vortices of equal strength that are turned on and off periodically so that one is on when the other is off, known as the blinking vortices, rotate around a common axis in a stepwise manner but induce chaos in nearby regions. On the other hand, if there are four of more vortices present, the vortex motion itself is generally chaotic. It should be noted that there are also nonchaotic equilibrium solutions of four or more vortices forming what is called a vortex crystal.

Information about chaotic particle motion is obtained by studying Poincaré sections, examining associated stable and unstable manifolds, and investigating the existence of chaotic maps such as the horseshoe map.

3.5 Atmospheric vortices

Atmospheric vortices are driven by temperature gradients, Earth's rotation (Coriolis force), spatial landscape variations, and instabilities. For example, temperature differences between the equator and the poles and Earth's rotation lead to large scale vortices such as the trade winds (Hadley cell), the jet streams, and the polar vortex (Fig. 13). Semi-annual temperature oscillations are responsible for the Indian monsoons. Daily oscillations cause land- and sea-breezes. Landscape variations can cause urban-rural wind flows and mountain-valley circulations.

Instabilities are often responsible for large cyclonic vortices. *Barotropic instability* results from large horizontal velocity gradients, and has been deemed responsible for disturbances over the Sahara region that occasionally intensify into tropical cyclones. *Baroclinic instability*, which occurs when temperature advection is superposed on a velocity field, can lead to cyclonic vortices at the front between air of polar origin and that of tropical origin. The *inertial or centrifugal instability* occurs when air flows around high pressure systems and the pressure gradient force is not large enough to balance the centripetal acceleration and the Coriolis effect.

Vortices also form on other planets with an atmosphere. On Mars dust devils

are quite common. They are about 10-50 times larger than the ones on Earth and can carry high voltage electric fields caused by the rubbing of dust grains against each other. Jupiter's characteristic spots are extremely large storm vortices. The Great Red Spot is a vortex spanning twice the diameter of the Earth. Unlike the low pressure terrestrial storms and hurricanes, the Great Red Spot is a high-pressure system that has been stable for more than 300 years. Other vortices on Jupiter decay and vanish, such as the White Ovals, three large anticyclones which merged into one within two years. Recent computer simulations predict that many of Jupiter's vortices will merge and disappear in the next decade. As a result, mixing of heat across zones will decay and the planet's temperature is predicted to increase.

Numerical simulations of the atmosphere are expensive due to the large number of parameters and the relatively small scales that need to be resolved. For climate models and medium range forecast models, the governing 3D compressible Euler Equations are simplified using the hydrostatic approximation (in which only the pressure gradient and the gravitational forces are retained in the vertical momentum equation) and the anelastic approximation (in which $\mathrm{d}\rho/\mathrm{d}t$ is neglected), to obtain the Primitive Equations. Additional vertical averaging yields the Shallow Water Equations. One big hurdle is to accurately incorporate the effect of clouds, which is significant and is usually treated using subgrid models.

3.6 Vortices in superfluids and superconductors

At temperatures below 2.2 K, liquid helium is a superfluid, meaning that it acts essentially like a fluid with zero viscosity governed by the Euler Equations. The fluid is irrotational except for extremely thin vortex filaments, which are formed by quantum mechanical processes. Since the vortices cannot end in the interior of the flow, they can be generated only at the surface or they nucleate as vortex rings inside the fluid. As an example, if a cylindrical container with helium is rotated sufficiently fast, vortex lines attached to both ends of the container appear. These quantum vortices have discrete values of circulation ($= nh/m$, where $h =$ Planck's constant, $m =$ mass of helium atom, $n =$ integer), core sizes of about 1 Angstrom (roughly the diameter of a single hydrogen atom) and move without viscosity.

Similarly, certain types of materials lose their electric resistance at low temperatures and become superconductors. One distinguishes type I superconductors (most pure metals) from type II superconductors (alloys). Using the Ginzburg-Landau theory it has been predicted that in type II superconductors a lattice of vortex filaments forms, each carrying a quantized amount of magnetic flux. This was subsequently confirmed by experimental observation. More precisely, for temperatures T below a critical value T_c, there are three regions corresponding to increasing values of the magnetic field (Fig. 14). At low magnetic fields $H < H_{c1}$ no vortices exist (superconducting phase). At intermediate values $H_{c1} < H < H_{c2}$ the magnetic field penetrates the superconductor in the form of quantized vortices, also called flux lines (mixed phase). The values $H_{c1,c2}$ are determined by the London penetration depth λ which measures the

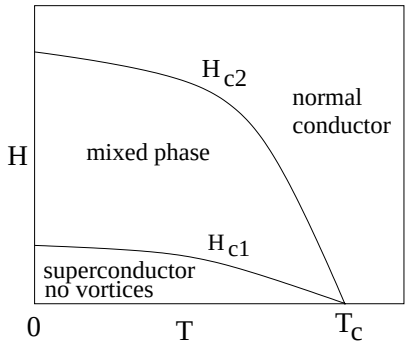

Figure 14: Superconductor phase dependence on magnetic field H and temperature T.

electromagnetic response of the superconductor. With increasing magnetic field the density of flux lines increases until the vortex cores overlap when the upper critical field H_{c_2} is reached, beyond which one recovers the normal metallic state (normal conductor).

When an external current density $\mathbf{j}$ is applied to the vortex system, the flux lines start to move under the action of the Lorentz force. As a result, a dissipating electric field $\mathbf{E}$ appears that is parallel to $\mathbf{j}$, and the superconducting property of dissipation-free current flow is lost. In order to recover the desired property of dissipation-free flow, flux lines have to be pinned, for example by introducing inhomogeneities and structural defects. For a given pinning force, flux lines remain pinned as long as the current density stays below a critical value. A major research objective is to optimize the pinning force in order to preserve superconductivity at larger current densities.

4. Numerical Vortex Methods

Many numerical methods used to compute fluid flow are *Eulerian* schemes based on a fixed mesh, such as finite difference, finite element and spectral methods, commonly used for example in atmosphere and ocean modelling. This section briefly describes alternative vorticity-tracking methods used to simulate incompressible inviscid vortex flows, and concludes with some extensions to viscous flows. The premise of these methods is that since the fluid velocity is determined by the vorticity through the Biot-Savart Law (Eq. 6), it suffices to track only that portion of the fluid carrying nonzero vorticity. This region is often much smaller than the total fluid volume, and computational efficiency is gained. Numerical vortex methods are typically *Lagrangian*, that is, the computational elements move with the fluid velocity.

4.1 Point vortex approximation in 2D

To compute the evolution of a vorticity distribution $\omega(\mathbf{x}, t)$ in 2D, the simplest approach is to approximate the vorticity by a set of point vortices at $\mathbf{x}_j(t)$ with circulation Γ_j and evolve them under their self-induced motion. The values Γ_j are an estimate of the initial circulation around $\mathbf{x}_j(0)$. The vortex positions

$\mathbf{x}_j(t)$ evolve in the induced velocity field

$$\frac{d\mathbf{x}_j}{dt} = \sum_{\substack{k=1 \\ k\neq j}}^{N} \Gamma_k \mathbf{K}_{2d}(\mathbf{x}_j - \mathbf{x}_k) \ , \tag{10}$$

where the exclusion $k \neq j$ accounts for the fact that a point vortex induces zero velocity on itself. The solution to the system of ordinary differential equations (10) can be obtained using any method such as Runge Kutta or Adams-Bashforth.

The point vortex approximation can be written in Hamiltonian form

$$\frac{dx_j}{dt} = -\frac{1}{\Gamma_j}\frac{\partial H}{\partial y_j} \ , \quad \frac{dy_j}{dt} = \frac{1}{\Gamma_j}\frac{\partial H}{\partial x_j} \ , \tag{11}$$

where the Hamiltonian

$$H(x,y) = \frac{1}{4\pi}\sum_{j=1}^{N}\sum_{\substack{k=1 \\ k>j}}^{N} \Gamma_j\Gamma_k \log\left[(x_j - x_k)^2 + (y_j - y_k)^2\right] \tag{12}$$

is conserved along fluid particles, $\mathrm{d}H/\mathrm{d}t = 0$. The method also conserves the fluid circulation and the linear and angular momenta.

Ideally, the solution to (10) should converge as $N \to \infty$ to the solution of the Euler Equations. This is true for smooth vorticity distributions, but for singular distributions such as a vortex sheet, the situation is more complicated. The vortex sheet, a curve in the plane, develops a singularity in finite time at which the curvature becomes unbounded at a point. The point vortex approximation converges before the singularity formation time, provided the growth of spurious roundoff error due to Kelvin-Helmholtz instability is suppressed using a filter. However, past the singularity formation time, the point vortex approximation no longer converges.

The general approach is to replace the singular kernel $\mathbf{K}_{2d}$ by a regularization $\mathbf{K}_{2d}^{\delta}$, such as

$$K_{2d}^{\delta} = \frac{1}{2\pi}\frac{-y\mathbf{i} + x\mathbf{j}}{|\mathbf{x}|^2 + \delta^2} \tag{13a}$$

$$K_{2d}^{\delta} = \frac{1}{2\pi}\frac{-y\mathbf{i} + x\mathbf{j}}{|\mathbf{x}|^2}\left(1 - e^{-|\mathbf{x}|^2/\delta^2}\right) \tag{13b}$$

where δ is a numerical parameter. The regularization amounts to replacing the delta-function vorticity of a point vortex by an approximate delta-function. In order to recover the solution to the Euler Equations it is necessary to study the limit $N \to \infty, \delta \to 0$. For smooth vorticity distributions, this process converges. For vortex sheet initial data, there is evidence of convergence, but details of the limiting behaviour remain under investigation. Regularized solutions with fixed value δ and vortex sheet initial data are shown in Figs. 6 and 15. Figure 6 shows the onset of the Kelvin Helmholtz instability in a periodically perturbed flat

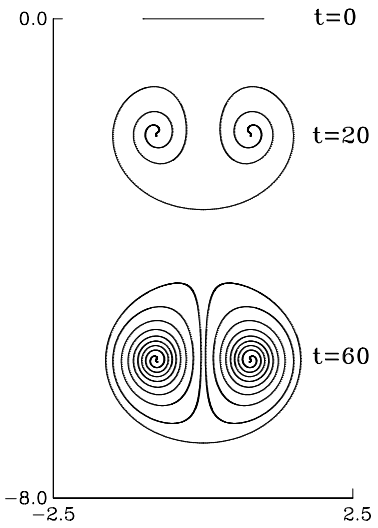

Figure 15: Computed evolution of an elliptically loaded flat vortex sheet.

vortex sheet. Figure 15 shows the rollup of an elliptically loaded flat vortex sheet that models the evolution of an aircraft wake (see Fig. 7). The correspondence between the two-dimensional simulation and the three-dimensional wake is made by replacing the spatial coordinate in the aircraft's line of flight by a time coordinate.

4.2 Contour dynamics in 2D

Consider a planar patch of constant vorticity ω_o bounded by a curve $\mathbf{x}(s,t), 0 \leq s \leq L$, moving in inviscid, incompressible flow. In view of Kelvin's Theorem and Eq (5), the vorticity in the patch remains constant and equal to ω_o for all time, and the patch area remains constant. Only the patch boundary moves. The velocity at a point $\mathbf{x}(\alpha,t)$ on the boundary can be written as a line integral over the boundary:

$$\frac{d\mathbf{x}}{dt} = -\frac{\omega_o}{2\pi}\int_C \log|\mathbf{x}-\mathbf{x}(s,t)|\frac{\partial \mathbf{x}}{\partial s}ds \ . \tag{14}$$

The contour dynamics method consists of approximating a given vorticity distribution by a superposition of vortex patches, and moving their boundaries according to Eq (14). This method has been applied to compute the evolution of single vortex patches and shear layers, and to geophysical flows. Typically, filamentation occurs: the patch develops thin filaments which increase the boundary length significantly and thereby the computational expense. The approach generally taken is to remove the thin filaments at several times throughout the computation, which is referred to as contour surgery. The contour dynamics approach as well as the point vortex approximation have also been generalized to treat quasigeostrophic flows.

4.3 Vortex filament methods in 3D

Vortex simulations in 3D differ from 2D in that the stretching term in Eq (4) needs to be incorporated. The vortex filament method approximates the fluid vorticity by a finite number of filaments whose circulation remains constant in time. Each filament is marked by computational meshpoints which move with the regularized induced velocity. The regularization is necessary to prevent the infinite self-induced velocities of curved vortex filaments. As in 2D, this method automatically conserves circulation. Vorticity stretching is accounted for by the stretching between computational meshpoints. As the filament length increases, more meshpoints are typically introduced to keep it resolved. Also, the number of filaments can be increased throughout the simulation to maintain resolution.

4.4 Viscous vortex methods

While inviscid models are expected to approximate small viscosity fluids well far from boundaries, near boundaries, where vortex shedding is an inherently viscous mechanism, it is important to incorporate effects of viscosity. The first methods to do so used operator splitting in which inviscid and viscous terms of the Navier-Stokes equations were solved in a sequential manner. In each timestep, the computational elements would first be convected, and then they would be diffused by a random walk scheme. The particle strength exchange method, introduced more recently, does not rely on operator splitting and has better accuracy. The particle position and vorticity evolve simultaneously, and viscous diffusion is accounted for in a consistent manner.

Vortex dynamics continues to be a source of interesting problems of theoretical and practical importance. In particular, much remains to be learned to better understand turbulence and the transition to turbulence, a process dominated by deterministic vortex dynamics.

References

References [13,21] are recommended as elementary introduction to vortex flows. Reference [22] presents beautiful and instructive flow visualizations. Comprehensive treatments of incompressible fluid dynamics are given in References [4,7,12,18], for compressible flow see [1]. Reference [8] gives an overview of numerical vortex methods. Special topics are addressed in [2] (atmosphere), [3,15,17] (point vortex motion and chaos), [5,9] (superfluids and superconductors), [6] (turbulence theory using statistical mechanics), [11] (vortex reconnection), [14] (theory for Euler and Navier-Stokes Equations), [16] (contour dynamics), [19] (vortex rings), and [20] (aircraft trailing vortices). Reference [10] includes survey articles on various topics.

[1] Anderson, J. D. (1990), Modern Compressible Flow with Historical Perspective. 2nd ed, New York: Mc Graw-Hill Publishing Company.

[2] Andrews, D. G., Holton, J. R., Leovy, C. B. (1987), Middle Atmosphere Dynamics. Orlando: Academic Press.

[3] Aref, H. (1983), Integrable, chaotic, and turbulent vortex motion in two-dimensional flows, *Ann. Rev. Fluid Mech.* **15**, 345–89.

[4] Batchelor, G. K. (1967), An Introduction to Fluid Dynamics. Cambridge: Cambridge University Press.

[5] Blatter, G., Feigel'man, M. V., Geshkenbein, V. B., Larkin, A. I. & Vinokur V. M. (1994), Vortices in high-temperature superconductors, *Rev. Mod. Phys.* **66** (4), 1125–388.

[6] Chorin, A.J. (1994), Vorticity and Turbulence, New York: Springer Verlag.

[7] Chorin, A. J. & Marsden, J. E. (1992), A Mathematical Introduction to Fluid Mechanics. 3rd ed, New York: Springer Verlag.

[8] Cottet, G.-H. & Koumoutsakos, P. D. (2000), Vortex Methods: Theory and Practice. Cambridge: Cambridge University Press.

[9] Donnelly R. J. (1991), Quantized Vortices in Helium II. Cambridge: Cambridge University Press.

[10] Green, S. I. (ed) (1995), Fluid Vortices. Kluwer Academic Publishers, Dordrecht.

[11] Kida, S. & Takaoka, M. (1994), Vortex reconnection, *Annu. Rev. Fluid Mech.* **26**, 169–89.

[12] Lamb, H. (1932), Hydrodynamics. 6th ed, New York: Dover.

[13] Lugt, H. J. (1983), Vortex Flow in Nature and Technology. New York: Wiley.

[14] Majda A. J. & Bertozzi A. L. (2002), Vorticity and Incompressible Flow. Cambridge: Cambridge University Press.

[15] Newton, P. K. (2001), The N-Vortex Problem: Analytical Techniques. New York: Springer Verlag.

[16] Pullin, D. I. (1992), Contour dynamics methods, Ann. Rev. Fluid Mech. 24, 89–115.

[17] Ottino, J. M. (1989), The Kinematics of Mixing: Stretching, Chaos, and Transport. Cambridge: Cambridge University Press.

[18] Saffman, P. G. (1992), Vortex Dynamics. Cambridge: Cambridge University Press.

[19] Shariff, K. & Leonard, A. (1992), Vortex rings, Ann. Rev. Fluid Mech. 24, 235–79.

[20] Spalart, P. R. (1998), Airplane trailing vortices, Ann. Rev. Fluid Mech. 30, 107–38.

[21] Tritton, D. J. (1988), Physical Fluid Dynamics. 2nd ed, Oxford: Clarendon Press.

[22] van Dyke, M. (1982), Album of Fluid Motion. Stanford: The Parabolic Press.

Monika Nitsche
Department of Mathematics and Statistics
University of New Mexico
Albuquerque, NM 87131-1141
nitsche@math.unm.edu